JOURNAL OF MATERIALS SCIENCE 25 (1990) 2549–2556

Mechanical and magnetic properties of the rapidly quenched Cu_2MnAl

YOSHIO SAKKA
National Research Institute for Metals, 2-3-12 Nakameguro, Meguro-ku, Tokyo 153, Japan
MORIHIKO NAKAMURA
National Research Institute for Metals, 1-2-1 Sengen, Tsukuba, Ibaraki 305, Japan

Rapidly solidified Cu_2MnAl ribbons were fabricated by the chill-block melt-spinning technique as a function of rotation speed of an iron roller. The rapidly quenched ribbons were relatively ductile, and the total strain at failure for the bend test increased with increasing rotation speed of the roller. The effect of rapid quenching on long-range ordering in Cu_2MnAl alloy was studied by X-ray diffraction. The decomposition characteristics during isothermal ageing at temperatures between 350 and 600° C were also examined by X-ray diffraction, magnetization and Vickers hardness measurements. The decomposition reaction at temperatures below 400° C was $Cu_2MnAl \rightarrow \gamma\text{-}Cu_9Al_4 + T\text{-}Cu_3Mn_2Al + \beta\text{-}Mn$. However, at temperatures between 500 and 600° C, Cu_2MnAl decomposed into a new $L2_1$ type Cu_2MnAl and β-Mn, and further annealing caused the appearance of $\gamma\text{-}Cu_9Al_4$. The decomposition rate of the rapidly quenched ribbons was faster than that of the water-quenched alloy.

1. Introduction

Intermetallic compounds have been expected to be advanced materials because of their unique mechanical, electrical and magnetic properties. However, the application of intermetallic compounds has been limited mainly by their brittleness. Much effort has been expended to improve the workability of intermetallic compounds. The melt-quenching technique is one of the best methods of improving mechanical properties.

The Heusler alloy Cu_2MnAl quenched from the Al region (approximately 850° C) has the ordered structure $L2_1$ [1] and is known to be brittle [2]. Cu_2MnAl with structure $L2_1$ is transformed into the ordered structure B2 and into the disordered bcc (Al) during heating at temperatures of 620 ± 20 and 780 ± 10° C, respectively [1]. The metastable phases are expected to be quenched by rapid quenching from the liquid and improvement of the mechanical properties is also expected [3, 4].

At temperatures lower than 650° C, the $L2_1$ phase is metastable and decomposes into three phases: β-Mn, $\gamma\text{-}Cu_9Al_4$ and $T\text{-}Cu_3Mn_2Al$. A number of studies concerning the decomposition process of the Cu–Mn–Al alloys has been carried out [5–11]. It is known that mechanical and magnetic properties change during isothermal ageing [6].

In the present study, the rapid quenching technique was applied to the Cu_2MnAl alloy and its mechanical properties were examined. The decomposition process at temperatures between 350 and 600° C were examined by changes in hardness and magnetization. The decomposition rate of the rapidly quenched ribbon was compared with that of the water-quenched alloy.

2. Experimental details

Commercially pure manganese, aluminium and copper were melted in a high-frequency furnace under an argon atmosphere. The alloy was subsequently heat treated for 2 h at 850° C and rapidly quenched in water. The atomic fraction determined by chemical analysis was $Cu_{2.01}Mn_{1.01}Al$, which is nearly equal to Cu_2MnAl. A charge of approximately 3 g was melted in a quartz crucible using a platinum furnace at 1400° C. The molten material was ejected through a nozzle of diameter 0.9 cm on to the rotating iron wheel, 8 cm diameter, by the aid of a rapid increase in argon pressure in the silica crucible.

The mechanical properties of the as-quenched ribbons were examined by micro-Vickers hardness measurement and a simple bending test. The micro-Vickers hardness was conducted at a load of 100 gf and 5 measurements were averaged. The long-range order parameters of the as-rapidly quenched ribbons were examined by X-ray diffraction using filtered Cu$K\alpha$ radiation. The variation of magnetization with induction up to 14 kOe was measured using a vibrating sample magnetometer.

The water-quenched alloys and the rapidly quenched ribbons were annealed at temperatures between 350 and 600° C for 5 min to 200 h *in vacuo*. The decomposition processes were examined by X-ray diffraction measurements, changes in magnetization and in micro-Vickers hardness, where the measurements were carried out on the wheel side of the rapidly quenched ribbon because the hardness was different between the wheel side and the upper side, and the values of the upper side were variable.

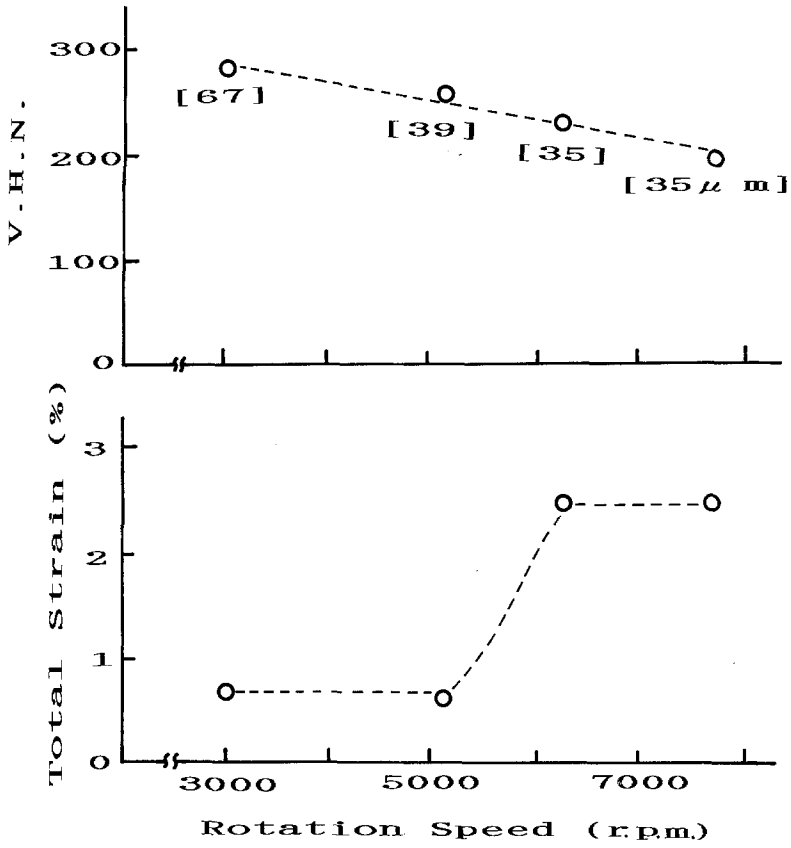

Figure 1 (a) Micro-Vickers hardness and (b) the total strain at failure as a function of the rotation speed under an argon pressure of 0.7 kg cm^{-2}, where the values in brackets denote the ribbon thickness.

3. Results and discussion

3.1. As-rapidly quenched ribbons

The rapidly quenched ribbons were obtained under conditions of rotation speed 3000 to 7700 r.p.m. and an argon pressure of 0.5 to 1.0 kg cm^{-2}. Fig. 1 shows the micro-Vickers hardness of the wheel side and the total strain at failure as a function of the rotation speed under an argon pressure of 0.7 kg cm^{-2}. The values in brackets shown in Fig. 1a denote the ribbon thickness (μm) determined from scanning electron micrographs. The thickness of the rapidly quenched ribbons decreased as the rotation speed increased. The total strain at failure, ε, for the bend test was calculated from the minimum bend radius, r, and the ribbon thickness, t, as follows [12, 13]

$$\varepsilon = t/(2r + t).$$

The total strain at failure increased with increasing rotation speed up to 6200 r.p.m. The improvement of the mechanical properties is considered to be mainly due to the following two reasons. One is the microstructural change. The Heusler alloy Cu_2MnAl with $L2_1$ structure is generally brittle, while the single crystal of Cu_2MnAl can be easily deformed in compression in the fixed directions [14]. The Heusler alloy wires produced by the in-rotating-water-spinning-process are also easily deformed owing to the bamboo structure which is composed of many single-crystals elongated to the wire axis [15]. Figs 2a and b show examples of the fractured surfaces of the ribbons fabricated under conditions in a fixed argon pressure of 0.7 kg cm^{-2} and a rotation speed of 3000 and 6200 r.p.m., respectively. The bamboo structure was partially observed for the rapidly quenched ribbons at a high rotation speed, as is seen in Fig. 2b. Therefore, improvement of the mechanical properties might be caused partly by improvement of microstructure.

Another possibility is considered to be the result of the quenching of the disordered phase. In the bcc

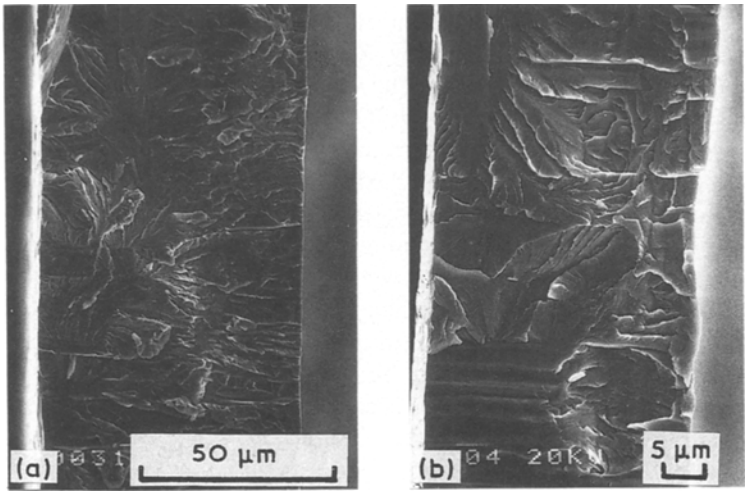

Figure 2 Scanning electron micrographs of the fractured surface of rapidly quenched ribbons with rotation speeds of (a) 3000 r.p.m. and (b) 6200 r.p.m.

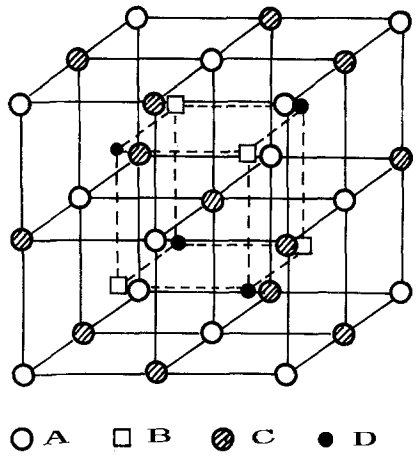

Figure 3 bcc type sublattice structure.

structure, lattice points are generally separated into four sublattices as shown in Fig. 3. In the $L2_1$ structure of Cu_2MnAl, the sites of the sublattices A and C are occupied by copper atoms, and the lattice sites of the sublattice B (or D) are occupied by aluminium atoms, while those of the sublattice D (or B) are occupied by manganese atoms. In the B2 structure, the sublattice sites of B and D are randomly occupied by aluminium or manganese atoms [16].

The following Bragg reflections appear on the X-ray diffraction pattern depending on the structure types [16].

1. h, k, l odd:

$$F_{hkl} = 4\,[(f_A - f_C)^2 + (f_B - f_D)^2]^{1/2}$$

2. h, k, l even and $(h + k + l)/2 = 2n + 1$:

$$F_{hkl} = 4(f_A - f_B + f_C - f_D)$$

3. h, k, l even and $(h + k + l)/2 = 2n$:

$$F_{hkl} = 4(f_A + f_B + f_C + f_D),$$

where f_A, f_B, f_C, f_D denote the atomic scattering amplitudes of atoms occupying the sublattices A, B, C, D.

TABLE I The superstructural intensities of the reflections (1 1 1) and (2 0 0) normalized to the intensity of the (2 2 0) reflection for the wheel side of the rapidly quenched ribbons, where the values in parentheses denote those of the upper side of the ribbons

Rotation speed (r.p.m.)	$10^2(J_{111}/J_{220})$	$10^2(J_{200}/J_{220})$
3000	3.3(0)	4.8(22.4)
6200	2.8(4.1)	4.6(6.5)
7700	2.5(4.0)	2.6(4.6)

The intensities of the reflections of the types 1 and 2 are functions of the degree of atomic order of $L2_1$ structure and B2 structure, respectively. Table I shows the superstructural intensities of the reflections (1 1 1) and (2 0 0) normalized to the intensity of the reflection (2 2 0) for the wheel side of Cu_2MnAl ribbons obtained as a function of rotation speed, where the values in parentheses denote those of the upper side of the ribbons. Fig. 4 shows the temperature dependences of the intensities of the Bragg reflections of (1 1 1) and (2 0 0) normalized to the intensity of the reflection (2 2 0) obtained by Soltys [16], where the straight lines denote the data of the wheel side of the rapidly quenched ribbons shown in Table I. The rapidly quenched ribbons show the partially disordered structure. Therefore, improvement of the mechanical properties is at least partly attributable to the disordered phases.

The normalized intensities of (1 1 1) and (2 0 0) of the upper side of the Cu_2MnAl ribbons at a rotation speed of 3000 r.p.m. are 0 and 22.4, respectively, as seen in Table I. These results indicate that the preferred grain growth occurred in the [0 0 1] axis at the lower rotation speed of 3000 r.p.m. The preferred grain growth axis is consistent with the preferred growth axis of the columnar grains of Cu_2MnAl ingot

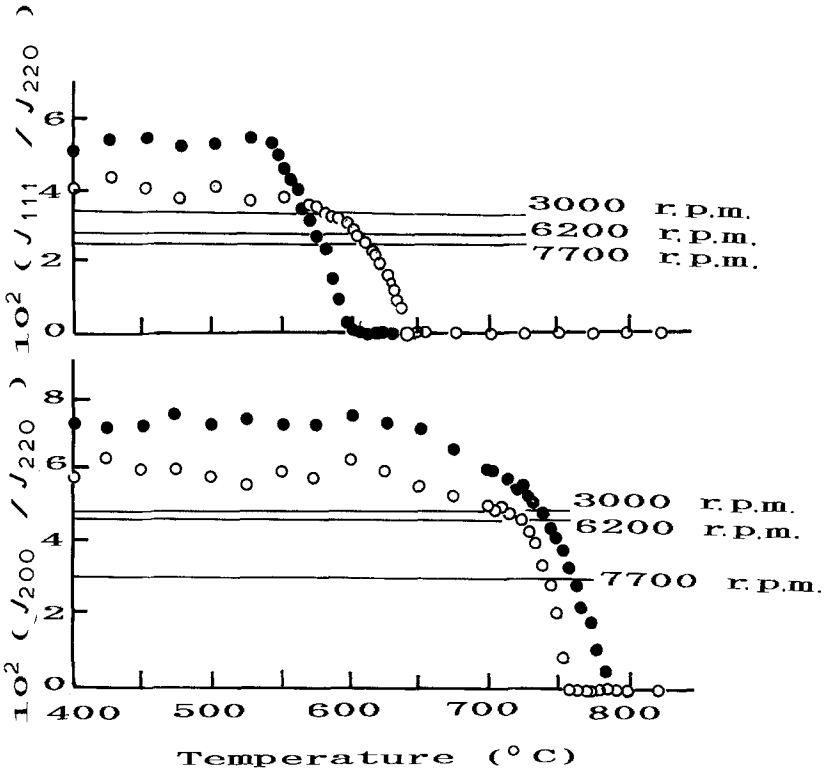

Figure 4 Temperature dependences of the intensities of the Bragg reflections of (1 1 1) and (2 0 0) normalized to the intensity of the (2 2 0) reflection. The straight lines denote the data of the wheel side of the rapidly quenched ribbons and the plots were obtained from Soltys [16]; (○) decreasing and (●) increasing temperature, respectively.

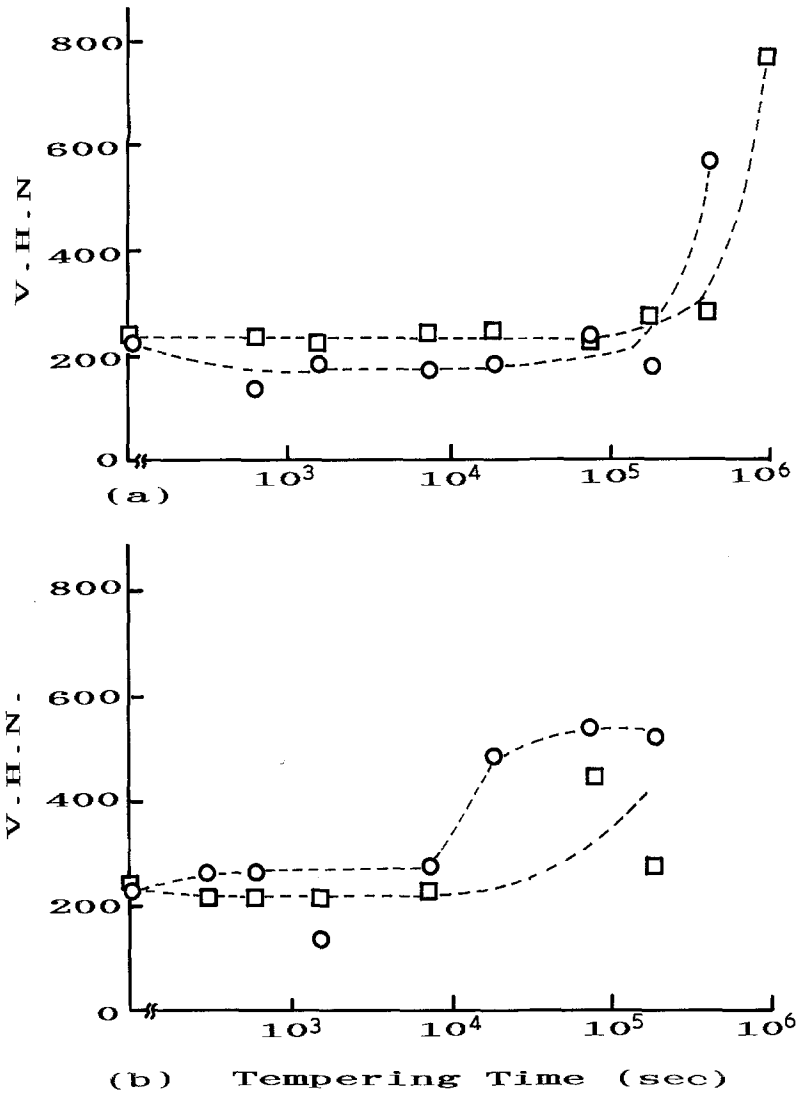

Figure 5 The relation between tempering time and Vickers hardness. (○) Rapidly quenched ribbon, (□) water-quenched alloy. (a) 350° C, (b) 400° C, (d) 500° C and (e) 600° C.

[2]. The preferred orientation is not observed when the rotation speed was above 6200 r.p.m. However, the amount of disordered phase of the upper side is smaller than that of the wheel side because of the difference in the quenching rate.

3.2. Decomposition characteristics

Isothermal annealings at 350, 400, 500 and 600° C were carried out for the rapidly quenched ribbons at a rotation speed of 6200 r.p.m. and for the water-quenched alloys. Figs 5a to d show the relation between tempering time and Vickers hardness. Figs 6a to d show the relation between tempering time and saturation magnetization. The decomposition characteristics of the two kinds of sample seem similar except for the decomposition rate. However, the decomposition characteristics at temperatures below 400° C are different from those at temperatures above 500° C.

First the decomposition characteristics of the rapidly quenched ribbons fabricated at a rotation speed of 6200 r.p.m. will be considered, and the decomposition rate of the two kinds of samples will be discussed.

3.2.1. Decomposition of rapidly quenched ribbon annealed at 350 and 400° C

The Vickers hardness and the saturation magnetization of the rapidly quenched ribbon at 350° C have constant values within the duration time of 50 h as seen in Figs 5a and 6a. However, a decrease in saturation magnetization and an increase in Vickers hardness can be seen when the annealing time exceeds 50 h. Fig. 7a shows the X-ray diffraction patterns of the rapidly quenched ribbons annealed at 350° C. The slight increase in T-Cu_3Mn_2Al, γ-Cu_9Al_4 and β-Mn phases are observed after annealing for 50 h. A significant increase in T-Cu_3Mn_2Al, γ-Cu_9Al_4 and β-Mn phases is observed and at the same time the Bragg reflections of the $L2_1$ phase disappear after annealing for 100 h.

Similar annealing-time dependences of the Vickers hardness and the magnetization of rapidly quenched ribbons are observed at 400° C as seen in Figs 5b and 6b. However, the duration time when the Vickers hardness increase and the saturation magnetization decrease is shorter than at 350° C. Fig. 7b shows the X-ray diffraction patterns after annealing at 400° C. After 20 h annealing, T-Cu_3Mn_2Al, γ-Cu_9Al_4 and β-Mn phases appear and at the same time the $L2_1$ phase disappears.

The decomposition reaction at 350 and 400° C is considered to be as follows

$$Cu_2MnAl \rightarrow \gamma\text{-}Cu_9Al_4 + \text{T-}Cu_3Mn_2Al + \beta\text{-Mn}.$$

3.2.2. Decomposition of rapidly quenched ribbons annealed at 500 and 600° C

As seen in Figs 6c and d, the saturation magnetization firstly decreases and then begins to increase as tempering

Figure 5 Continued

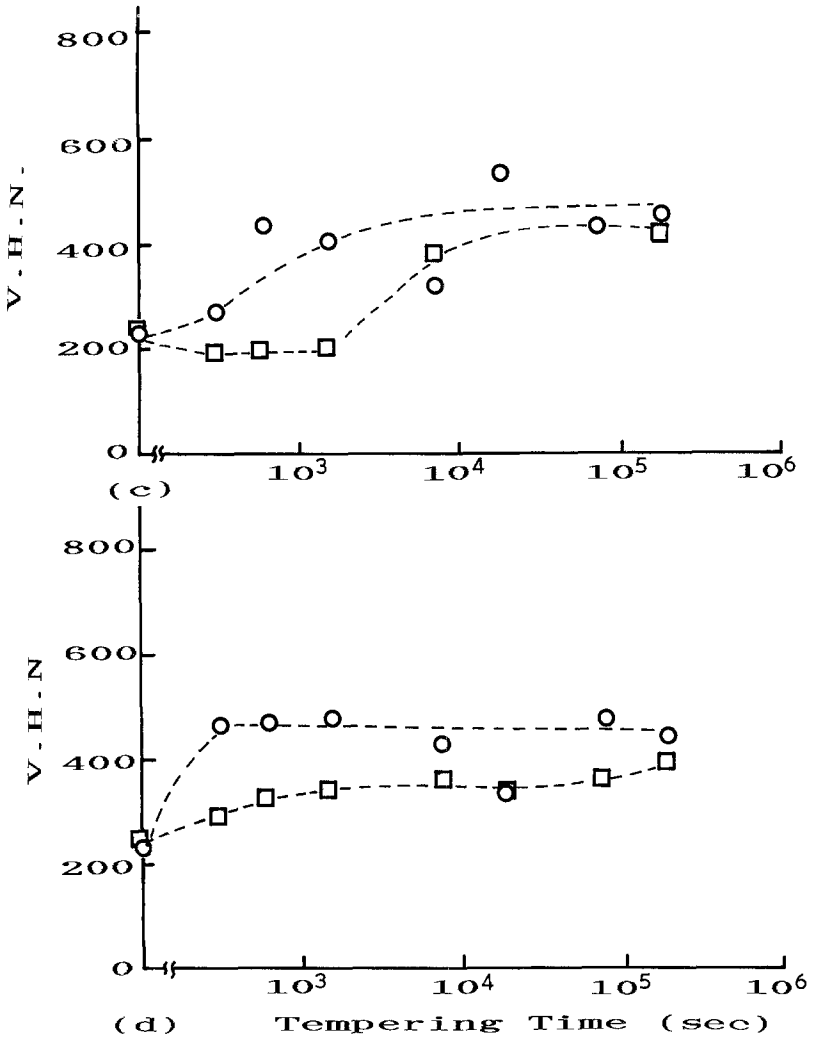

time increases. This result suggests the appearance of another new Cu_2MnAl phase as reported by Kozubski and Soltys [7, 10]. Fig. 7c shows the X-ray diffraction patterns of the rapidly quenched ribbon annealed at 500° C. Initially, the $L2_1$ phase is broadened, β-Mn phases appear and simultaneously a new phase precipitates after 25 min annealing. On further annealing, the γ-Cu_9Al_4 phases can be observed. The structure of the new phase is $L2_1$ type [7], while the lattice parameter is smaller than that of the initial $L2_1$ phase. (The peak angle is shifted to higher angle.)

Fig. 7d shows the X-ray diffraction patterns of the rapidly quenched ribbon annealed at 600° C, The $L2_1$ phase disappears and the new $L2_1$ phase and β-Mn phase appear after annealing for 10 min. The γ-Cu_9Al_4 phase is faintly observed after annealing for 51 h.

The decomposition reaction at temperatures of 500 and 600° C is considered initially as follows

$$Cu_2MnAl \rightarrow Cu_2MnAl \text{ (new phase)} + \beta\text{-Mn}$$

and further annealing causes the following reaction

$$Cu_2MnAl \text{ (new phase)} + \beta\text{-Mn} \rightarrow Cu_2MnAl \text{ (new phase)} + \beta\text{-Mn} + \gamma\text{-}Cu_9Al_4.$$

3.2.3. Comparison of decomposition characteristics of rapidly quenched ribbon with water-quenched alloy

The decomposition characteristics of the two samples are similar as seen in Figs 5 and 6. However, the decomposition rate of the rapidly quenched ribbons is faster than that of the water-quenched alloy. Fig. 8 shows the tempering time (incubation time [6]) when the saturation magnetization begins to decrease and the hardness begins to increase as a function of the reciprocal annealing temperature. The incubation time obtained from the saturation magnetization is in fair agreement with that obtained from hardness. This result indicates that both saturation magnetization and hardness are exactly related to structure change.

Soltys *et al.* [11] reported that the heterogeneous precipitation predominated with an activation energy of 46 kcal mol^{-1}, which was obtained by electrical resistance measurement at temperatures up to 467° C, and that above this temperature a new mechanism came into play with a lower activation energy. Yamane *et al.* [6] successfully obtained the temperature of the change in the character of the decomposition process for the $Cu_{2.05}Mn_{0.92}Al$ alloy, where they determined the temperature by the intercept point of two straight lines on a graph of the relation between incubation time (hardness begins to increase) and the reciprocal of ageing temperature. As is discussed in the previous section, the decomposition characteristics differ between the temperatures above 500° C and below 400° C. The activation energies of the rapidly quenched ribbon and the water-quenched alloy at temperatures below 400° C are estimated to be $\sim$ 51 and 43 kcal mol^{-1}, respectively. These values are

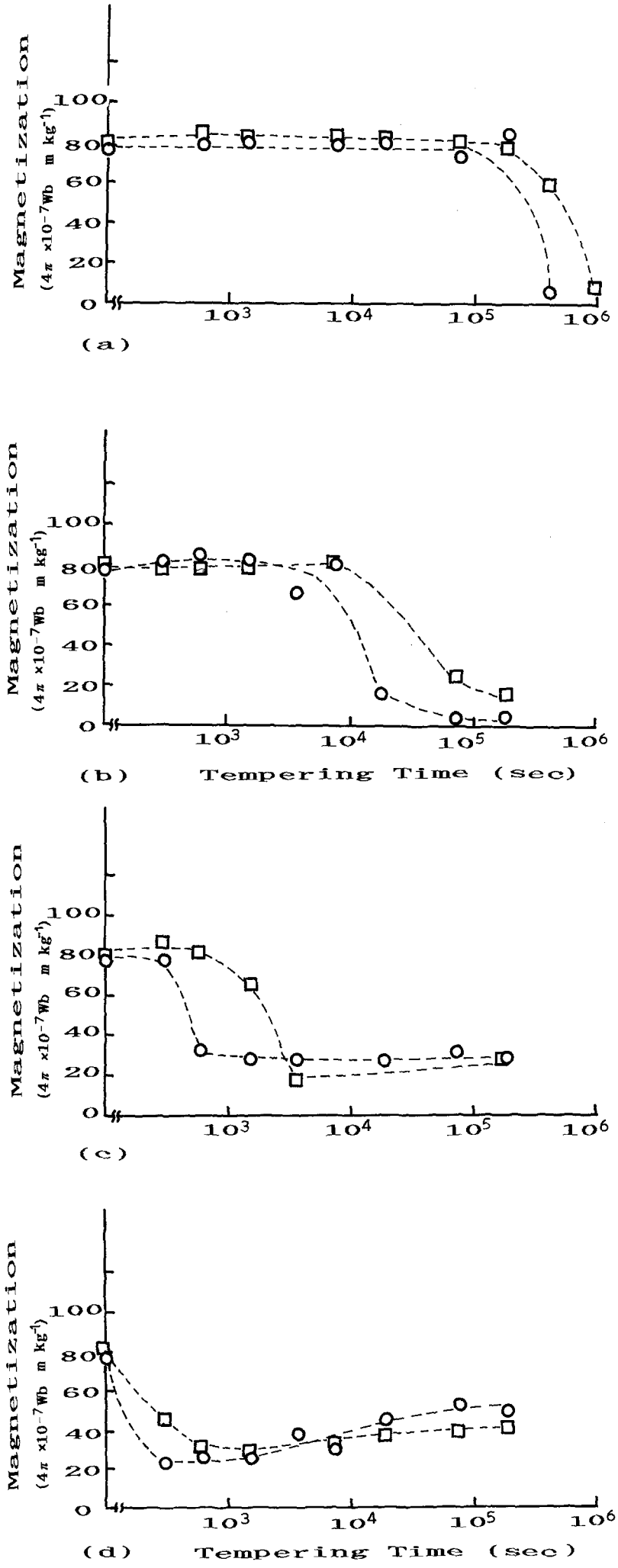

Figure 6 The relation between tempering time and magnetization. (○) Rapidly quenched ribbon, (□) water-quenched alloy. (a) 350° C, (b) 400° C, (c) 500° C and (e) 600° C.

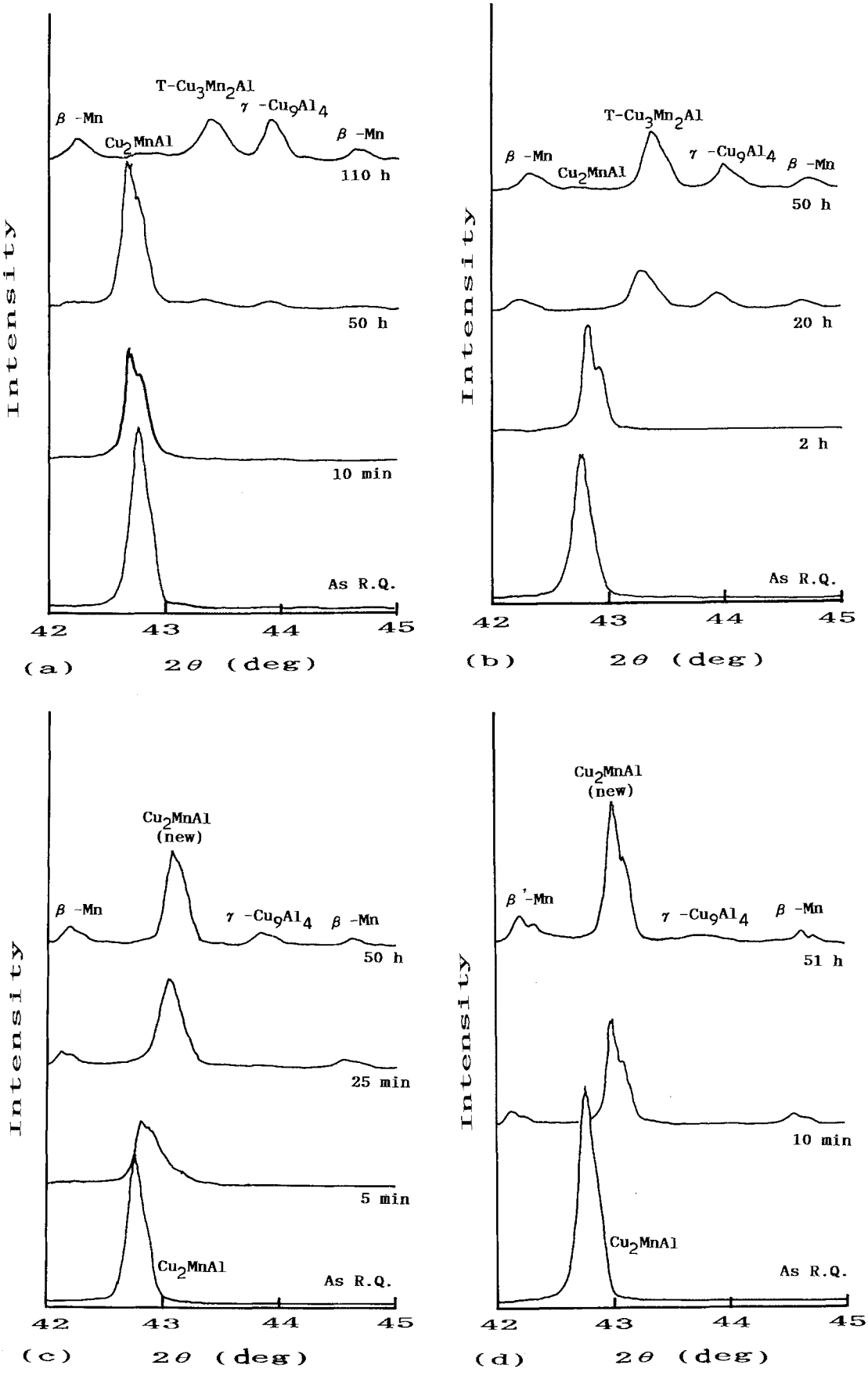

Figure 7 X-ray diffraction patterns of the rapidly quenched ribbons annealed at (a) 350° C, (b) 400° C, (c) 500° C and (d) 600° C.

close to 46 kcal mol^{-1} [11]. Therefore, a similar mechanism of decomposition, which is heterogeneous precipitation, seems to be predominant for the two samples at temperatures below 400° C. Above 500° C, homogeneous precipitation, with a lower activation energy, as seen in Fig. 8, seems to come into play, as suggested by Soltys *et al.* [11].

4. Conclusion

The rapidly quenched Cu_2MnAl ribbons were fabricated under various rotation speeds (iron wheel diameter 8 cm) of 3000 to 7000 r.p.m. and an argon pressure of 0.5 to 1.0 kg cm^{-2}. A decrease in hardness and increase in the strain at failure are observed with increase in the rotation speed of the roller. These

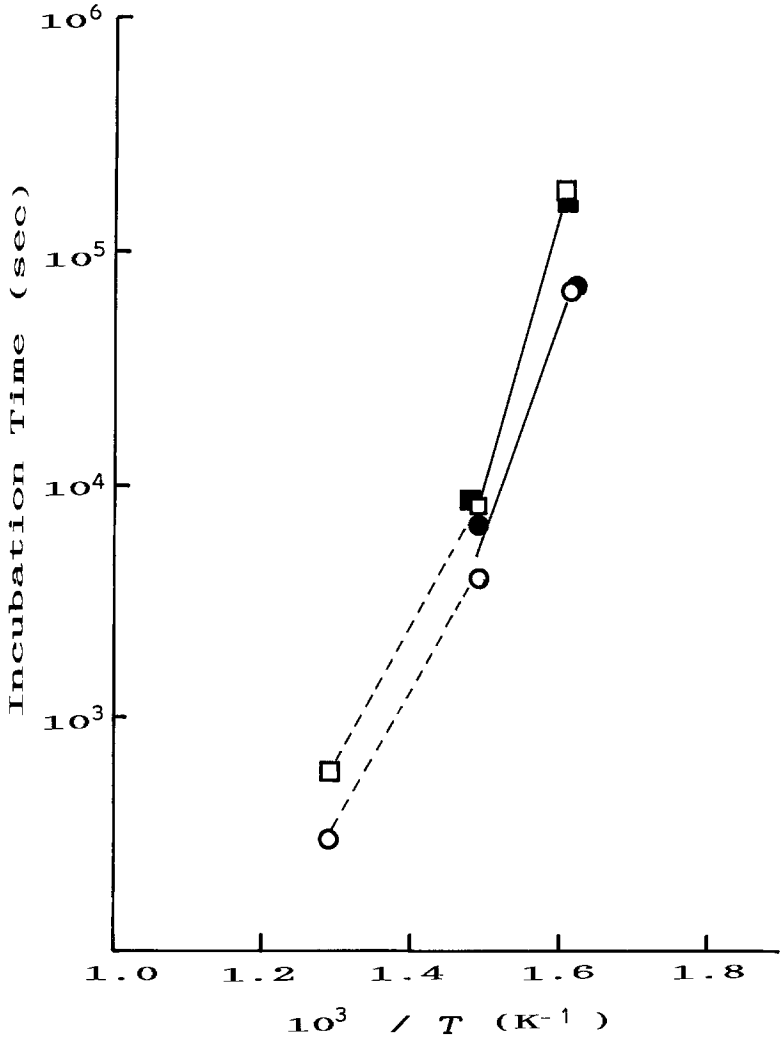

Figure 8 Temperature dependences of the tempering time when (●, ■) hardness begins to increase and (○, □) magnetization begins to decrease. (●, ○) Rapidly quenched ribbons, (■, □) water-quenched alloy.

results are considered to be due to the improvement of microstructure and the quenching of the disordered phases. The preferred grain growth occurred in the [0 0 1] axis at the lower rotation speed of 3000 r.p.m.

The decomposition characteristics were examined for the rapidly quenched ribbon and the water-quenched alloy by X-ray diffraction, magnetization and hardness measurements. The decomposition rate of the rapidly quenched ribbon was faster than that of the water-quenched alloy. However, the decomposition features of both samples were similar as follows. At temperatures of 350 and 400° C, the decomposition reaction is expressed as $Cu_2MnAl \rightarrow \gamma\text{-}Cu_9Al_4 + T\text{-}Cu_3Mn_2Al + \beta\text{-}Mn$. At temperatures of 500 and 600° C, the decomposition reactions may be expressed initially as $Cu_2MnAl \rightarrow Cu_2MnAl$ (new phase) + β-Mn, and further tempering caused further appearance of $\gamma\text{-}Cu_9Al_4$.

Acknowledgements

The authors thank Drs K. Hoshimoto, H. Maeda and Y. Kawabe for their helpful suggestions and discussions.

References

1. M. BOUCHARD and G. THOMAS, *Acta. Metall.* **32** (1975) 1485.
2. M. L. GREEN and G. Y. CHIN, *Met. Trans.* **6A** (1975) 1118.
3. A. INOUE, T. MASUMOTO and H. TOMIOKA, *J. Mater. Sci.* **19** (1984) 3097.
4. Y. SAKKA, M. NAKAMURA and K. HOSHIMOTO, *ibid.* **24** (1989) 4331.
5. B. DUBOIS and D. CHEVEREAU, *ibid.* **14** (1979) 2296.
6. T. YAMANE, H. OKAMOTO and J. TAKAHASHI, *Z. Metallkde* **71** (1980) 813.
7. R.KOZUBSKI and J. SOLTYS, *J. Mater. Sci.* **17** (1982) 1441.
8. *Idem, ibid.* **18** (1983) 1689.
9. R. KOZUBSKI, J. SOLTYS and R. KUZIAK, *ibid.*, **18** (1983) 3079.
10. R. KOZUBSKI and J. SOLTYS, *J. Mater. Sci. Lett.* **2** (1983) 141.
11. J. SOLTYS, M. STEFANIAK and J. HOLENDER, *Phil. Mag. B* **49** (1984) 151.
12. D. J. GAYDOSH, R. W. JECH and R. H. TITRAN, *J. Mater. Sci. Lett.* **4** (1985) 138.
13. G. E. DIETER,"Mechanical Metallurgy", 2nd Edn. (McGraw-Hill, New York, 1976) p. 681.
14. Y. UMAKOSHI, M. YAMAGUCHI and T. YAMANE, *Acta Metall.* **32** (1984) 649.
15. Y. ONO, I. OHNAKA and I. YAMAUCHI, *J. Jpn Inst. Metals* **51** (1987) 755 (in Japanese).
16. J. SOLTYS, *Phys. Status Solidi (a)* **63** (1981) 401.

Received 15 February
and accepted 24 August 1989.